CALCULATED PHOTOELECTRON PITCH ANGLE AND ENERGY SPECTRA

by

G. P. Mantas*

and

S. A. Bowhill

Department of Electrical Engineering
University of Illinois
Urbana, Illinois 61801

(NASA-CR-140040) CALCULATED PHOTOELECTRON PITCH ANGLE AND ENERGY SPECTRA (Illinois Univ.) 49 p HC $5.50 CSCL 04A

N74-33864

Unclas
G3/13 49588

*Present Address: Department of Geology and Geophysics, Yale University, New Haven, Connecticut 06520

ABSTRACT

Calculations of the steady-state photoelectron energy and angular distribution in the altitude region between 120 and 1000 km are presented. The distribution is found to be isotropic at all altitudes below 250 km, while above this altitude anisotropies in both pitch angle and energy are found. The isotropy found in the angular distribution below 250 km implies that photoelectron transport below 250 km is insignificant, while the angular anisotropy found above this altitude implies a net photoelectron current in the upward direction. The energy anisotropy above 500 km arises from the selective backscattering of the low energy photoelectron population of the upward flux component by Coulomb collisions with the ambient ions. The total photoelectron flux attains its maximum value between about 40 and 70 km above the altitude at which the photoelectron production rate is maximum. The displacement of the maximum of the equilibrium flux is attributed to an increasing (with altitude) photoelectron lifetime. Photoelectrons at altitudes above that where the flux is maximum are on the average more energetic than those below that altitude. The flux of photoelectrons escaping to the protonosphere at dawn was found to be 2.6×10^8 $cm^{-2} \cdot sec^{-1}$, while the escaping flux at noon was found to be 1.5×10^8 cm^{-2} sec^{-1}. The corresponding escaping energy fluxes are: 4.4×10^9 eV cm^{-2} sec^{-1} and 2.7×10^9 eV cm^{-2} sec^{-1}.

1. INTRODUCTION

To study dayglow emissions, electron and ion temperatures, predawn airglow intensity and electron temperature enhancements, exospheric neutral particle temperatures, etc. one needs to know the equilibrium energy spectrum of the photoelectrons (energetic electrons) that constitute the energy source of these phenomena. Several theoretical studies (Hoegy et al., 1965; Nisbet, 1968; Henry and McElroy, 1968; Dalgarno et al., 1969; Rees et al., 1969; Banks and Nagy, 1970; Nagy and Banks, 1970; Takayanagy and Itikawa, 1970; Cicerone and Bowhill, 1971a; Dalgarno and Lejeune, 1971) have progressively improved our knowledge of the energy spectrum of photoelectrons in the ionosphere. In parallel, experimental studies (Shea et al., 1968; Yngvesson and Perkins, 1968; Rao and Maier, 1970; Heikkila, 1970; Evans and Gastman, 1970; Doering et al., 1970; Cicerone and Bowhill, 1971b; Knudsen and Sharp, 1972; Galperin et al., 1972) have provided valuable data for comparison with the theoretical results.

In a recent review Cicerone et al. (1973) have found that at high altitudes differences of about a factor of two are found among photoelectron fluxes calculated by different theoretical methods. Although these differences can be eliminated within the existing theoretical framework, experimental techniques (Doering et al., 1973; Hays and Sharp, 1973) have improved substantially in resolution and accuracy to warrant more detailed theoretical calculations than hitherto undertaken. In a previous paper (Mantas 1974) a detailed theoretical formulation of the problem of photoelectron thermalization and transport

in the ionosphere was presented. In the present paper we use that theory to calculate the steady-state pitch angle and energy distribution of photoelectrons for two ionospheric models appropriate for conditions prevailing over Arecibo (18.4°N, 67°W) on December 24, 1968 at dawn (0703 hours, solar zenith angle $\chi \simeq 90°$), and on June 26, 1968 at noon (1225 hours, $\chi \simeq 0°$).

The boundary conditions for the photoelectron thermalization and transport equation have been discussed by Mantas (1974). In the present calculations we have assumed (upper boundary condition) that there is no photoelectron flux incident upon the ionosphere at 1000 km. At 120 km (lower boundary) a partially reflecting boundary, with a reflection coefficient of 0.6, was assumed. It was found, however, that the lower boundary condition has no significant effect on the solution because at this altitude transport is insignificant. The contribution of a non-zero downward flux at the upper boundary can be calculated separately and added to the present calculations.

2. IONOSPHERIC MODELS, PHOTOELECTRON PRODUCTION RATES, AND CROSS SECTIONS

2.1 Neutral Atmospheres.

The neutral particle densities used in these calculations have been obtained from the Bates (1959) model atmosphere as elaborated by Stein and Walker (1965) and Walker (1965). The neutral gas densities at 120 km and the other parameters of the Bates model have been obtained from a combination of theoretical considerations and temperature data from Arecibo at the indicated times (R. J. Cicerone, Private communication, 1972) The neutral atmosphere exospheric temperature for the sunrise model is 884 Kelvin, while that of the noon model is 1114 Kelvin.

2.2 Charged Particle Densities.

The electron density profiles have been obtained from Thomson scatter observations over Arecibo at the indicated times (R. J. Cicerone, Private communication, 1972). The electron and neutral atmosphere densities can be found in Mantas (1973) . Since all ions are assumed to be singly charged and their mass is much larger than the electron mass, all electron-ion collisions are characterized by the same collision cross section and no distinction is made between different kinds of ions.

2.3 Primary Photoelectron Energy Spectra.

Energy spectra of the primary photoelectron production rates, at selected altitudes, for the sunrise model are shown in Figure 1. These spectra have been calculated by R. S. Stolarski (private communication, 1972) using the EUV flux measurements of Hinteregger (1970) and the photo-ionization cross sections reviewed by Stolarski and Johnson (1972). The pitch angle distribution of the primary photoelectron production rate

is assumed to be that given by Mariani (1964).

2.4 Cross Sections

We have used the empirical formula

$$\sigma_j(E) = \frac{q_o A_j}{W_j^2}\left(1 - \frac{W_j}{E}\right)^{\xi_j}\left(\frac{W_j}{E}\right)^{\omega_j} \qquad (1)$$

proposed by Green and Dutta (1967), to represent the excitation cross sections. In equation (1) E is the electron energy, W_j is the excitation potential of the state j, $q_o = 6.51 \times 10^{-14}$ cm^2 eV^2, and A_j, ξ_j, ω_j are dimensionless parameters obtained by fitting (1) to experimentally determined cross sections. For the excitation of atomic oxygen we have used values for the parameters of (1) suggested by R. S. Stolarski (private communication, 1972). For molecular nitrogen, molecular oxygen, and helium we have used the values given by Stolarski et al. (1967), Watson et al. (1967), and Jusick et al. (1967), updated to more recent cross section measurements by Jobe et al. (1967), Burns et al. (1969), McConkey and Simpson (1969), Simpson and McConkey (1969), Stanton and St. John (1969), Brinkman and Trajmar (1970), Sheridan et al. (1971), McConkey and Woolsey (1969), and Skubenich (1968). The probability densities $P_\ell^i(E',E)$ (see Mantas 1974) for the energy distribution of the post-collision electrons in electron-neutral ionizing collisions have been constructed from the differential cross sections given by Khare (1969) and Dalgarno and Lejeune (1971). The total ionization cross sections have been taken from the review paper of Kieffer and Dunn (1966). A listing of the values of the parameters of (1) is given by Mantas (1973).

3. RESULTS AND DISCUSSION

3.1 Photoelectron Flux Pitch Angle and Energy Spectra at Dawn

In Figures 2a through 2d, the logarithm of the photoelectron flux ($\log_{10} 2\pi\ \Phi(h,E,\mu)$) is plotted at selected altitudes. For negative values of the direction variable ($\mu < 0$) the electrons are moving in the downward direction along the magnetic field lines, while for positive values they move in the upward direction. Note that the flux shown in these figures has been integrated over the azimuthal angle ϕ; the quantity $2\pi\ \Phi(h,E,\mu)$, therefore, represents the flux over a pitch angle cosine interval $\Delta\mu$ and not over a unit solid angle.

Intercomparison of these figures reveals variations of the flux with each of the independent variables. For altitudes below about 250 km $\Phi(h,E,\mu)$ is isotropic (independent of μ). For altitudes above 250 km more electrons are moving in the upward than in the downward direction — the anisotropy becoming increasingly larger with increasing altitude. It is important to note that most of the flux variation occurs in the small interval $-0.25 \leq \mu \leq 0.25$ or, in terms of the pitch angle, in the region between about 75 and 105 degrees. Outside this region the dependence of Φ upon μ is weaker. Above 800 km the angular dependence is much stronger; however, in this region most of the variation is introduced through the somewhat unrealistic upper boundary condition that no downward flux is present at the 1000 km level. Although at certain times of the year conditions exist where no flux from the conjugate ionosphere is present, some of the upward flux will be scattered downward at altitudes higher than 1000 km, and thus constitute a nonzero upper boundary condition.

An estimate of the reflection coefficient at the upper boundary will be given later.

Now we turn our attention upon the examination of the photoelectron flux energy spectrum. Examination of Figures 2a through 2c reveals considerable structure of $\Phi(h,E,\mu)$ with respect to the energy variable. For altitudes below about 250 km the local energy variation is much smoother than that above this altitude. A comparison of Figure 2a with the primary photoelectron spectrum at low altitudes (see Figure 1) reveals that the energy spectrum of the steady-state photoelectron flux is much smoother than the energy spectrum of the primary production rate. The prominent peaks of the primary spectra are absent in the equilibrium flux spectra. The wide maximum in the energy region between 20 and 65 eV, in the primary spectra, is substantially reduced. The deep and wide minimum, in the primary spectra, in the energy about 10 eV, has disappeared completely and the flux has a negative slope in the energy interval between 10 and 20 eV, while the production spectra have a large positive slope in this interval. For altitudes below about 250 km (see Figure 2a) the steady state photoelectron flux spectra show an increasingly larger slope, with decreasing energy below about 40 eV (small local variations in the slope are neglected). At about 10 eV the photoelectron flux begins to increase rapidly with decreasing energy. This increase is interrupted at about 5 eV, and begins again, at a much higher rate, for energies below about 2.5 eV.

For altitudes at about 250 km and above, the most prominent features of the primary photoelectron spectra are also present in the photoelectron flux spectra, though less prominent in the latter case. The substantial

structure found in the production spectra in the region below about 20 eV is absent in the flux spectra. A careful examination of the Figures 2b through 2c reveals many interesting variations of the photoelectron flux with altitude, pitch angle, and energy. In addition to the prominent upward-downward anisotropy that has been mentioned, the following important features should be noticed:

(a) The steep rise in the flux spectrum observed at altitudes below 250 km at about 2 eV is absent from the energy spectra at about 300 km and above.

(b) For altitudes at about 450 km and above, in the energy region below about 5 eV, the upward moving flux decreases with decreasing energy the decrease becoming larger with increasing altitude.

(c) The features present in the spectra around 25 eV, for a fixed direction (μ = constant), become smoother with increasing altitude above 300 km.

(d) The smoothness of the spectrum features at a fixed altitude increases with decreasing absolute value of the direction variable μ.

These results can be interpreted in physical terms as follows. At low altitudes, due to the higher concentration of the neutral atmospheric constituents relative to the thermal electron concentration, the photoelectron flux energy spectrum is mainly determined by inelastic collisions. For altitudes above about 300 km the photoelectron-thermal electron interaction becomes increasingly important with increasing altitude.

The pitch angle isotropy of the electron flux spectra below about 250 km shows that electron transport at these altitudes is negligible. On the other hand, the increasing pitch angle anisotropy with altitude above 300 km shows that electron transport increases in importance as the altitude increases. The importance of transport at high altitudes can also be deduced from the fact that the electron flux changes little with increasing altitude above 400 km, although the photoelectron production rate decreases rapidly. Therefore, to interpret the characteristics of the electron flux spectra and obtain a qualitative evaluation of the validity of the solution, one must consider that most of the electrons found at high altitudes are produced in the altitude region between 250 and 350 km and are subsequently transported to higher altitudes by spiralling around the magnetic field lines.

The energy lost by an electron in its upward motion through the ambient electron gas is a function of the distance it traverses and its initial energy. If we neglect elastic scattering by the ambient ions the distance traversed by an electron in reaching certain altitude, say 700 km, is inversely proportional to the cosine of its pitch angle. Although elastic scattering smears the distance traversed by the electrons found at the same altitude in the same pitch angle interval, on the average one would expect that electrons with large pitch angles, say in a small interval around 70 degrees, would have traversed longer distances, in reaching the said altitude, than electrons with smaller pitch angles. If the electrons in both pitch angle intervals had originated from the same altitude and had the same initial energy, upon reaching a high altitude the electrons with large pitch angles would have lost more of

their initial energy than those with smaller pitch angles.

From these considerations one would expect that prominent features in the photoelectron production spectra, such as the peaks around 25 eV due to the absorption of the He II lines of the solar EUV, if they appear in the steady-state electron flux spectra should increase in width and shift towards lower energies with increasing altitude and pitch angle. The broadening and shift towards lower energies of these features as $|\mu| \to 0$ is clearly seen in Figure 2c.

It should be also observed that at high altitudes the slope $\frac{\partial}{\partial E} \Phi(h,E,\mu)$ of the energy spectrum of the upward ($\mu>0$) electron flux component at the low energy limit ($E < 5eV$) is positive, while that of the downward flux ($\mu < 0$) is negative. This behavior indicates that the upward electron flux component loses low energy electrons at a higher rate than it gains, while the opposite holds for the downward flux component. Since at high altitudes photoelectrons are losing energy mainly to the thermal electron gas and are redistributed in pitch angle by Coulomb collisions with the ambient ions, the interplay of these two processes must, to a large extent, determine the shape of the spectrum at the low energy limit. The rate at which a fast electron is losing energy to the thermal electron gas with distance is, approximately, inversely proportional to its energy. And the cross section for Coulomb collisions is inversely proportional to the square of the energy. Energy loss to the thermal electron gas, therefore, constrains low energy photoelectrons from reaching high altitudes and, in addition, Coulomb collisions with ions selectively backscatter low energy electrons from the upward to the downward flux component. These two processes operate

on the downward flux component in the same manner. However, due to the larger number of upward moving electrons, Coulomb collisions give rise to a net transfer of electrons from the upward to the downward flux component. Since the cross section for Coulomb collisions depends on the inverse square of the energy, low energy electrons are preferentially backscattered. The net effect of this process is reflected in the shape of the spectra in the low region and, as we shall see below, gives rise to an energy anisotropy between the upward and downward flux components.

3.2 Photoelectron Flux Energy Spectra at Dawn

Integration of $2\pi\ \Phi(h,E,\mu)$ over μ gives the number of electrons per unit energy interval crossing a sphere of unit surface in all directions per second. This quantity will be referred to as the total photoelectron flux energy spectrum and will be written as $\Phi^{\tau}(h,E)$. Thus

$$\Phi^{\tau}(h,E) = 2\pi \int_{-1}^{1} \Phi(z,E,\mu)d\mu = \Phi^{-}(h,E) + \Phi^{+}(h,E) \qquad (2)$$

where

$$\Phi^{-}(h,E) = 2\pi \int_{-1}^{0} \Phi(h,E,\mu)d\mu \qquad (2a)$$

represents the energy spectrum flux crossing the downward hemisphere, and

$$\Phi^{+}(h,E) = 2\pi \int_{0}^{1} \Phi(h,E,\mu)d\mu \qquad (2b)$$

represents the energy spectrum of the flux crossing the upward hemisphere.

The total photoelectron flux energy spectrum $\Phi^{\tau}(h,E)$ is shown in Figure 3. It should be noted that this surface is somewhat distorted because unequal altitude intervals have been plotted along the depth axis as if they were equal. For example $\Phi^{\tau}(h,E)$ has been evaluated at 9 altitudes in the altitude interval between 200 and 300 km, while in the interval between 300 and 400 km it has been evaluated at 7. The ratio of the intervals along the depth axis representing the altitude intervals from 200 to 300 km and from 300 to 400 km, is 9/7 instead of one. This distortion does not affect the accuracy of this figure, it should, however, be kept in mind when Figure 3 (and also Figures 5, 6 and 8) is examined. Figures 2a through 2c do not suffer from this distortion because, although $\Phi(h,E,\mu)$ was evaluated at unequal pitch angle cosine intervals, interpolation has been used to obtain values of $\Phi(h,E,\mu)$ at equal intervals along the μ (depth) axis before plotting.

A careful examination of Figure 3 shows that the sharp peak of the spectrum at about 25 eV becomes broader and shifts towards lower energies with increasing altitude as discussed previously. The spectrum is also seen to become smoother with increasing altitude above 300 km.

To obtain a quantitative view of the up-down energy anisotropy we evaluate the mean energies:

$$\overline{E^{-}}(h) = \frac{1}{\Phi^{-}(h)} \int_{1}^{100} E\Phi^{-}(h,E)dE \qquad (3a)$$

$$\overline{E^{+}}(h) = \frac{1}{\Phi^{+}(h)} \int_{1}^{100} E\Phi^{+}(h,E)dE \qquad (3b)$$

$$\overline{E_{\Phi}}(h) = \frac{1}{\Phi^{\tau}(h)} \int_{1}^{100} E\Phi^{\tau}(h,E)dE \qquad (3c)$$

where:

$$\Phi^{-}(h) = \int_{1}^{100} \Phi^{-}(h,E)dE \qquad (4a)$$

$$\Phi^{+}(h) = \int_{1}^{100} \Phi^{+}(h,E)dE \qquad (4b)$$

$$\Phi^{\tau}(h) = \int_{1}^{100} \Phi^{\tau}(h,E)dE \qquad (4c)$$

are the total number of electrons crossing a sphere of unit surface, at the altitude h per unit time interval, (a) in the downward direction, (b) in the upward direction, (c) in both directions.

The mean energies $\overline{E^{-}}(h)$ and $\overline{E^{+}}(h)$ are shown in Figure 4, together with the ratio $\overline{E^{+}}(h)/\overline{E^{-}}(h)$ and the mean energy $\overline{E_s}$ of the primary photoelectron spectrum (source). From this figure it can be seen that for altitudes above about 550 km the upward flux consists of more energetic electrons than the downward flux. This is exactly what one would expect in accordance with the arguments presented in the previous paragraphs. For altitudes between 250 and 550 km the downward flux is composed of slightly more energetic ($\overline{E^{-}} > \overline{E^{+}}$, by about 0.5 eV at most) electrons than the upward flux. Below 250 km energy isotropy is seen to prevail, as one would expect, due to the large number of collisions at low altitudes. The energy anisotropy at high altitudes is probably higher than that calculated here, since it is known that at high energies the elastic collision cross sections are strongly peaked in the forward direction, while we have assumed isotropic scattering for elastic collisions independently of the collision energy. The mean energy of the total photoelectron flux is found by integrating equation (3c). The curve for $\overline{E_\Phi}$ has not been plotted, since it follows closely the

curve for $\overline{E_T}$.

It is interesting to compare the mean energy $\overline{E_s}$ (source) of the photoelectron production rate with $\overline{E_\Phi} \approx \overline{E_T}$. For altitudes above 350 km $\overline{E_s}$ is approximately independent of altitude and has a value of about 18 eV. Below 350 km $\overline{E_s}$ rises rapidly with decreasing altitude to a value of about 41 eV at 170 km, while $\overline{E_\Phi}$ decreases with altitude from a value of about 17 eV at 1000 km to about 7 eV at 160 km. The large difference of about 17 eV at 1000 km to about 7 eV at 160 km. The large difference between $\overline{E_s}$ and $\overline{E_\Phi}$ at altitudes below 300 km indicates that the high energy rate as rapid as the rate of production. Above 300 km inelastic collisions cease to play the dominant role, and the equilibrium spectrum is shifted only slightly toward the low energy region, since elastic collisions with ions absorb no energy and photoelectron-thermal electron energy transfer is a slow process for photoelectron energies greater than few electron volts.

3.3 Photoelectron Flux Pitch Angle and Energy Spectra at Noon.

In the present and following subsections we present electron flux spectra for noontime conditions. We shall limit the discussion, however, only to pointing out what is new or different from the dawn model spectra. For details the interested reader should consult Mantas (1973).

The main difference in the input parameter of the two models consists of higher neutral and charged particle concentrations in the noon than in the dawn model. The F_2-layer thickness is larger in the noon than in dawn model, with a peak electron density of $10^6(cm^{-3})$ at about 400 km, while the maximum electron density in the dawn model is about $5X10^5$,

and the F_2-layer peak occurs at about 250 km. Another important difference is the higher primary photoelectron production rate, with a maximum at a lower altitude, in the noon than the dawn model. The maximum primary photoelectron production rate at noon is 3.2×10^3 (cm^{-3} sec^{-1}) at about 150 km, while that at dawn is 1.5×10^2(cm^{-3} sec^{-1}) at about 250 km.

The higher neutral and charged particle densities, and the lower altitude of the maximum primary photoelectron production rate in the noon model give rise to the following differences between the dawn and noon electron flux spectra:

a) The angular anisotropy at high altitudes at noontime is smaller than that at dawn.

b). The energy spectrum above 300 km at noon is smoother than the dawn spectrum.

c) The broadening and the shift towards lower energies of the prominent features of the spectrum, at fixed altitudes above 400 km, with decreasing $|\mu|$ is larger at noon than at dawn. The same is also true for the broadening and shifting of these features with increasing altitude for fixed values of μ.

d) The amplitude of the flux above 400 km at noon is smaller than that at dawn.

A better illustration of the upward-downward electron flux anisotropy at high altitudes is obtained by integrating the flux $\Phi(h,E,\mu)$ over all energies. The function

$$\Phi(h,\mu) = 2\pi \int_1^{100} \Phi(h,E,\mu)dE \qquad (5)$$

represents the total number of electrons, irrespective of their energy, in

the pitch angle cosine internal $d\mu$ about μ. This function is shown in Figure 5. It is interesting to note that the pitch angle dependence shown in this figure is in qualitative agreement with the single energy analytical results of Stolarski (1972). The rapid variation of the pitch angle distribution in the 90 degree region at high altitudes is clearly seen. It should be also observed that outside this region the upward flux component is almost isotropic.

In Figure 6 the total photoelectron flux energy spectrum $[\Phi^{\tau}(h,E)]$ at noon, defined by (2) is shown. Comparison of Figures 3 and 6 shows that the broad maximum between 200 and 300 km in the high energy region, seen in the dawn model, is barely present in the noon model. Another interesting characteristic to be noted is the very rapid transition in the smoothness of the noon spectrum at about 300 km. In the dawn spectrum (Figure 3) no such sharply defined transition altitude is found. Further comparison of these figures shows that the broadening and shift of the noon spectrum features, with increasing altitude, is larger than that for dawn. A more clear illustration of this effect is given in Figure 7 where the energy spectrum of the upward photoelectron flux at noon is shown. The prominent peak at 22.5 eV at 304 km is gradually broadened and shifted to about 20 eV as the altitude increases to 1000 km.

The effect of energy absorption by the thermal electron gas and the Coulomb scattering by the ions can be seen in the energy dependent attenuation of the flux with altitude. For example the flux amplitude in the energy region around 70 eV decreases only by about a factor of 2

as the altitude increases from 300 to 1000 km, while in the region around 5 eV it decreases by about a factor of 20 over the same altitude interval.

In Figure 8 the mean energy of the photoelectron flux at noon, as function of pitch angle and altitude, defined by

$$\bar{E}_{\Phi}(h,\mu) = \frac{2\pi}{\Phi(h,\mu)} \int_{1}^{100} E\, \Phi(h,E,\mu)\, dE, \qquad (6)$$

is shown. Below about 220 km the mean energy of the photoelectron flux is independent of altitude and pitch angle and has a value of about 8 eV. Between 220 and 400 km it is independent of pitch angle but rises rapidly with altitude to the value of 17 eV at 400 km. Above this altitude the mean energy is a function of both pitch angle and altitude, rising with altitude to about 18 eV at 1000 km for $\mu > 0$, while decreasing to about 14 eV for $\mu < 0$. The complicated structure of the mean energy demonstrates the importance of calculating the pitch angle distribution of the flux, since otherwise this structure cannot be revealed.

3.4 Integrated Photoelectron Fluxes.

The integrated photoelectron fluxes $\Phi^{-}(h)$, $\Phi^{+}(h)$, and $\Phi^{T}(h)$ defined by equations (4a, b, and c) are shown in Figure 9. The upward-downward electron flux anisotropy, noted previously, is clearly seen to persist down to about 250 km. There are three additional conclusions that can be drawn from the examination of this figure.

First, the steady-state photoelectron flux attains its maximum value at a higher altitude than that where the photoelectron production rate is maximum. In section 3.3 it was noted (see Mantas 1973) that

the photoelectron production rate for $\chi = 90°$ is maximum at about 250 km. From Figure 9 it is seen that for $\chi = 0°$ the total photoelectron flux is maximum at about 220 km, while for $\chi = 90°$ is maximum at about 290 km. Therefore, at noon the total flux attains its maximum value about 70 km above the altitude where the production rate is maximum. At dawn the displacement is 40 km. This displacement is not due to transport. This can be deduced from the observation that the photoelectron flux distribution is isotropic in pitch angle below about 250 km, which implies that there is no net photoelectron current below this altitude, and also, from the fact that the displacement is larger in the noon than in the dawn model, contrary to what one would expect if the displacement were due to transport. The cause of this displacement must, therefore, be sought elsewhere. The most likely cause is an altitude dependent photoelectron lifetime. To derive the photoelectron lifetime one would have to solve the time dependent transport equation, which at the present seems impractical. An indication that the displacement is due to this cause is given by the altitude dependence of the mean photoelectron energies. From Figures 4, 8 and 9 is seen that the photoelectron flux maximum occurs at exactly the same altitude as the altitude above which the mean photoelectron energy increases rapidly. In Figure 4 there appear to be two such changes; the altitude of the photoelectron flux maximum coincides with that of the upper change.

Second, the upward photoelectron flux above 500 km, and therefore the escape flux, is larger at dawn than at noon. With regard to this conclusion it should be noted that the upward flux at 1000 km at noon is lower than the maximum upward flux at 220 km by about a factor of 10, while

at dawn this factor is about 5. The stronger altitude dependence of the upward flux at noon is due to the larger column number density (neutral molecules and ions included) at noon than at dawn.

And third, the photoelectron flux below 250 km depends strongly upon the solar zenith angle, while above this altitude the dependence on χ is weak. Therefore, while comparison between measured and calculated fluxes below 250 km is difficult unless the solar zenith angles are the same, above 250 km meaningful comparisons between theory and experiment can be made even for different solar zenith angles.

3.5 Photoelectron Escape and Energy Input into the Protonosphere.

Above 700 km the upward photoelectron flux Φ^+ is seen (Figure 9) to change very little with altitude. This implies that very few of the electrons that reach this altitude are backscattered into the ionosphere while the majority escape to the protonosphere. To obtain an estimate of the backscattered fraction of photoelectrons we consider the rate of change with altitude of the ratio (Φ^-/Φ^+) at the base of the protonosphere. In the altitude interval 800 to 900 km we find (from Figure 9, $\chi = 90°$) that the altitude dependent reflection coefficient is about 5×10^{-5} (km^{-1}). If we assume that photoelectrons are reflected at the same rate in the first 1000 km above the base of the protonosphere, and beyond this altitude they are completely absorbed, the reflection coefficient R_b at the base of the protonosphere (h = 1000 km) is 0.05. This value of R_b is, at best, a rough estimate; it demonstrates, however, that most of the upward flux at high altitudes escapes to the protonosphere. In the examination of the differential flux spectra (Figures 2 through 2c)

we noticed that at high altitudes the backscattering probability is much higher for low than for high energy electrons. This implies that the reflection coefficient is energy dependent. The energy dependent reflection coefficient can be obtained from the energy spectra by arguments similar to those used above. However, our interest is not to calculate the reflection coefficient but simply to show that it is small, and proceed with the calculation of the escape flux.

The net number of photoelectrons per electron volt crossing a unit surface perpendicular to the z-axis (the direction of the magnetic field), in the direction of increasing z, per second, at the altitude h, is

$$\Phi_n(h,E) = 2\pi \int_{-1}^{1} \mu\, \Phi(h,E,\mu)d\mu \qquad (7)$$

where we have inserted the subscript n to distinguish the net flux parallel to the magnetic field line defined by (7) from $\Phi^{\tau}(h,E)$ defined by (2). Evaluation of (7) at h = 1000 km gives the energy spectrum of the escaping flux. A negative flux $\Phi_n(h,E)$ at 1000 km implies that a net number of electrons enter the ionosphere at the upper boundary. Integration of this equation over E at 1000 km gives 2.6 X 10^8 cm^{-2} sec^{-1} and 1.5 X 10^8 cm^{-2} sec^{-1} for the escaping electron fluxes at dawn and noon, respectively. Multiplying (7) by E and integrating over E at 1000 km we obtain 4.4 X 10^9 eV cm^{-2} sec^{-1} for the energy input rate into the protonosphere at dawn, and 2.7 X 10^9 eV cm^{-2} sec^{-1} for the energy input rate at noon. These energy input rates compare favorably with the downward conduction heat fluxes (Evans 1967; Evans and Mantas 1968) obtained from observed electron temperature gradients at high altitudes over Millstone Hill

4. COMPARISON WITH EXPERIMENT

Before we compare the present calculations with measured photoelectron flux energy spectra we like to point out that the theoretical energy spectra for $\chi = 0°$ shown in the following three figures have been recalculated. This was considered necessary in order to evaluate the effect of an error in the computer program which was found after most of the calculations had been performed. It was found that this error affected only the low energy region of the spectrum, especially in bringing out a more pronounced effect on the spectrum due to the vibrational excitation of N_2. Since it did not have any substantial effect elsewhere, nor did it affect the conclusions drawn from the previous calculations, it was deemed unnecessary to repeat all the calculations.

Before comparing the calculated spectra with experimental results we would like to point out the extent to which agreement can be expected. First, the energy resolution of the experimental results is not sufficient to confirm or disprove the finer structure of the energy sepctra found in our calculations. Therefore, find structure comparison must be by-passed until experimental data of the required degree of resolution become available. Second, the number of experiments is limited, being confined to altitudes below 300 km, where the fluxes depend strongly upon the solar zenith angle. An exception to this is the data of Galperin et al. (1972) which refer to altitudes above 300 km; however,

the absolute value of the fluxes measured in these experiments is questionable due to calibration problems. These authors have normalized their data to the results of Doering et al. (1970), at 300 km, in the energy region between 30-40 eV.

In Figure 10 the calculated photoelectron flux energy spectrum at 179 km is compared with the experimental data of Doering et al. (1970) and Knudsen and Sharp (1972) at 180 km. In the same figure we have also included the data by Galperin et al. (1972) at 250 km. The experimental data were given as electrons cm^{-2} eV^{-1} $ster^{-1}$ sec^{-1}; here we have multiplied these data by 4π to obtain total fluxes. No error is introduced by this, since our calculations have shown that the fluxes are uniformly distributed over all directions (isotropic) at this altitude. The agreement is excellent for energies above 5 eV. Below this energy there are only two data points at 4 eV. In the caluclated spectrum the slope changes sign at about 5 eV, while in the measured spectrum no such change is seen. However, a recent experiment by Hays and Sharp (1973) that covers the energy region below 5 eV clearly shows the change in the slope between 4 and 5 eV and the presence of a minimum at about 2.5 eV. The observed minimum is, however, much shallower than that in the calculated spectrum, indicating either insufficient experimental resolution, or an overestimated cross section for vibrational excitation of N_2. It should be noted, however, that the overestimate need not be large since only small change in the ratio of the inelastic to the elastic cross sections affects substantially the calculated spectrum.

In Figures 10-12 it is interesting to note that broad features in the calculated spectrum are also present in

the measured spectra. For example, in the energy region about 15 eV the measurements of Doering et al. (1970) definitely show structure; this is also true in the energy interval between 40 and 50 eV in the data of Knudsen and Sharp (1972). Since in both regions the calculated spectra also show broad features, the absence of the sharp peaks between 20 and 30 eV in the measured spectra indicates that the experimental resolution is not sufficient to resolve these peaks.

From Figure 9 it can be seen that the magnitude of the flux at 180 km and 250 km is approximately equal (for $\chi = 0°$). Therefore, it is not inappropriate to include the Cosmos 348 results at 250 km, by Galperin et al. (1972), in this comparison.

From this comparison we can see that the theory is in good agreement with experiment at the high energy region also. Between 30 and 60 eV the agreement is good. Above this energy the calculated spectrum is lower by a factor of 3, or less, depending on the energy. Above about 70 eV the calculated spectrum is changing little with energy, while the measured spectrum continues to decrease at a different rate, however, than that observed below 70 eV. The change in the slope of the measured spectrum rectrum reflects the change seen clearly in the calculated spectrum. Taking into account the fact that we have not included energies above 100 eV, it is expected that the calculated spectrum between 70 and 100 eV would be lower than the actual distribution. In this region the calculations can be extended straightforward to include energies above 100 eV. Such an extension would require only calculation of photoelectron production rates with energies above 100 eV, and extension of the collision cross sections over this energy region. Although an extension

that includes production above 100 eV will affect the energy spectrum everywhere, the energy regions that are expected to be mostly affected are the high and low energy regions, the first because cascading from energies above 100 eV would be nonzero, and the second, mostly through secondary low energy electron production by ionization.

In Figure 11 the calculated spectra are compared with the results of Knudsen and Sharp (1972) for several altitudes below 180 km. At altitudes above 140 km the agreement is fairly good; however, the change in the slope at about 5 eV, found in our calculations, does not appear in the data. We have already pointed out reasons for this discrepancy. The calculated spectrum at 121 km is lower than the observed. The disagreement at this altitude is not too large if we take into consideration the large solar zenith angle difference, and the fact that the calculations reprsent low solar activity conditions, while the data correspond to a higher level of solar activity.

In Figure 12 we compare calculated spectra at various altitudes with the measurements of Doering et al. (1970). Since the large solar zenith angle difference precludes detailed comparison, we shall compare only the shapes of the calculated and measured spectra. If we exclude the change in the sign of the slope of the spectrum at about 5 eV, which as we have noted has been observed in a more recent experiment, the agreement is good. It should be noted here that since the calculations are very sensitive to changes in the ratio of the inelastic to the elastic cross sections, the agreement shown in this figure can be substantially improved by small changes in the cross sections in future calculations.

5. CONCLUSIONS

Theoretical calculations of photoelectron flux energy spectra have revealed several important characteristics of the photoelectron distribution function, the most important of which are:

(a) The angular distribution of the photoelectron flux is isotropic at all altitudes below about 250 km. Above this altitude an upward-downward flux anisotropy is found which increases with altitude. This anisotropy gives rise to a larger upward flux component, and therefore a net photoelectron current in the upward direction.

(b) At altitudes above 550 km the mean energy of the upward flux component is larger than that of the downward component and changes very slowly with altitude. The mean energy of the downward flux component on the other hand decreases rapidly with altitude above 550 km. In the region between 250 and 550 km the mean energy of the downward flux is slightly larger than that of the downward component. Below this altitude energy, as well as angular, isotropy prevails.

(c) The total photoelectron flux attains its maximum value at altitudes higher than that where the production rate is maximum. Since transport has been found insignificant below 250 km this displacement has been attributed to an altitude increasing photoelectron lifetime. The altitude where the flux is maximum coincides with the altitude above which the mean photoelectron energy begins to rise rapidly with altitude. Therefore, photoelectrons at altitudes higher than that where the flux is maximum are on the average more energetic than those below this altitude.

(d) The total number of photoelectrons escaping to the protonosphere at dawn is larger than the number escaping at noon by about a factor of two. The same is also true with regard to the energy supplied to the protonosphere by these electrons.

ACKNOWLEDGEMENTS

The authors are indebted to Dr. R. J. Cicerone and Dr. R. S. Stolarski for the calculation of the primary photoelectron energy spectra and for providing the parameters for the excitation cross sections of atomic oxygen. This research has been supported by the National Science Foundation through Grant GA 36911X to the University of Illinois and by the National Aeronautics and Space Administration through Grant NGR 07-004-109 to Yale University.

REFERENCES

Banks, P. M. and Nagy, A. F. (1970). Concerning the influence of elastic scattering upon photoelectron transport and escape. J. Geophys. Res. 75, 1902-1910.

Bates, D. R. (1959). Some problems concerning the terrestrial atmosphere above the 100-km level. Proc. Roy. Soc.(London) A523, 451-462.

Brinkmann, R. T. and Trajmar, S. (1970). Electron impact excitation of N_2. Ann. Geophys. 26, 201-207.

Burns, D. J., Simpson, F. R., and McConkey, J. W. (1969). Absolute cross sections for electron excitation of the second positive bands of nitrogen. Jour. Phys. B. 2, 52-64.

Cicerone, R. J. and Bowhill, S. A. (1971a). Photoelectron fluxes in the ionosphere computed by a Monte Carlo method. Jour. Geophys. Res. 76, 8299-8317.

Cicerone, R. J. and Bowhill, S. A. (1971b). Photoelectron fluxes measured at Millstone Hill. Rad. Sci. 6, 957-966.

Cicerone, R. J., Swartz, W. E., Stolarski, R. S., Nagy, A. F., and Nisbet, J. S. (1973). Thermalization and transport of photoelectrons: A comparison of theoretical approaches. Jour. Geophys. Res. 78, 6709-6728.

Dalgarno, A., McElroy, M. B., and Stewart, A. I. (1969). Electron impact excitation of the dayglow. Jour. Atmos. Sci. 26, 753-762.

Dalgarno, A. and Lejeune, G. (1971). The absorption of electrons in atomic oxygen. Planet. Space Sci. 19, 1653-1667.

Doering, J. P., Fastie, W. G., and Feldman, P. D. (1970). Photoelectron excitation of N_2 in the day airglow. Jour. Geophys. Res. 75, 4787-4802.

Doering, J. P., Bostrom, C. O., and Armstrong, J. C. (1973). The photoelectron-spectrometer experiment on Atmosphere Explorer. Rad. Sci. 8, 387-392.

Evans, J. V. (1967). The heating of the protonosphere. Space Res. VIII, 717-727.

Evans, J. V. and Mantas, G. P. (1968). Thermal structure of the temperate latitude ionosphere. Jour. Atmos. Terr. Phys. 30, 563-577.

Evans, J. V. and Gastman, I. M. (1970). Detection of conjugate photoelectrons at Millstone Hill. Jour. Geophys. Res. 75, 807-815.

Galperin, Y. I.; Dymek, M.; Kutiev, I.; Mulyarchik, T. M.; Serafimov, K. B.; Shuiskaya, F. K.; and Wernik, A. (1972). Spectra of ionospheric photoelectrons and their transport from the conjugate ionosphere. Rept. Acad. Sci. USSR, Inst. Space Res., no. 107.

Green, A. E. S. and Dutta, S. K. (1967). Semi-empirical cross sections for electron impacts. Jour. Geophys. Res. 72, 3933-3941.

Hays, P. B. and Sharp, W. E. (1973). Twilight airglow: 1. Photoelectrons and [OI] 5577-angstrom radiation. Jour. Geophys. Res. 78, 1153-1166.

Heikkila, W. J. (1970). Photoelectron escape flux observations at mid-latitudes. Jour. Geophys. Res. 75, 4877-4879.

Henry, R. J. W. and McElroy, M. B. (1968). Photoelectrons in planetary atmospheres. The Atmosphere of Venus and Mars (Eds. J. C. Brandt and M. B. McElroy). Gordon and Breach, New York 251-285.

Hinteregger, H. E. (1970). The extreme ultraviolet solar spectrum and its variation during a solar cycle. Ann. Geophys. 216, 547-554.

Hoegy, W. R., Fournier, J. P., and Fontheim, E. G. (1965). Photoelectron energy distribution in the F region. Jour. Geophys. Res. 70, 5464-5467.

Jobe, J. D., Sharpton, F. A., and St. John, R. M. (1967). Apparent cross sections of N_2 for electron excitation of the second positive system. Jour. Opt. Soc. Amer. 57, 106-107.

Jusick, A. T.,Watson, C. E., Peterson, L. R., and Green, A. E. S. (1967). Electron impact cross sections for atmospheric species, 1. Helium. Jour. Geophys. Res. 72, 3943-3951.

Khare, S. P. (1969). Energy spectrum of the secondary electrons and the fluorescent efficiency of electrons in the 3914-Å band. Planet. Space Sci. 17, 1257-1268.

Kieffer, L. J. and Dunn, G. H. (1966). Electron impact ionization cross-section data for atoms, atomic ions, and diatomic molecules: 1. Experimental data. Rev. Mod. Phys. 38, 1-35.

Knudsen, W. C. and Sharp, G. W. (1972). Eclipse and noneclipse differential photoelectron flux. Jour. Geophys. Res. 77, 1221-1232.

Mantas, G. P. (1973). Ph.D. Thesis: Electron collision processes in the ionosphere. Aeron. Rep. No. 54, Univ. of Ill., Urbana-Champaign, Ill.

Mantas, G. P. (1974). Theory of Photoelectron thermalization and transport in the ionosphere. Planet. Space Sci. (in press).

Mariani, F. (1964). Pitch-angle distribution of the photoelectrons and the origin of the geomagnetic anomaly in the F_2 layer. Jour. Geophys. Res. 69, 556-560.

McConkey, J. W. and Simpson, F. R. (1969). Electron impact excitation of the $B^3\Pi_g$ state of N_2. Jour. Phys. B. 21, 923-929.

McConkey, J. W. and Woolsey, J. M. (1969). Excitation of O_2^+ bands by electron impact. Jour. Phys. B. 2, 529-533.

Nagy, A. F. and Banks, P. M. (1970). Photoelectron fluxes in the ionosphere. Jour. Geophys. Res. 75, 6260-6270.

Nisbet, J. S. (1968). Photoelectron escape from the ionosphere. Jour. Atmos. Terr. Phys. 30, 1257-1278.

Rao, B. C. N. and Maier, E. J. R. (1970). Photoelectron flux and protonospheric heating during the conjugate point sunrise. Jour. Geophys. Res. 75, 816-822.

Rees, M. H., Stewart, A. I., and Walker, J. C. G. (1969). Secondary electrons in aurora. Planet. Space Sci. 17, 1997-2008.

Shea, M. F., Sharp, R. D., and McElroy, M. B. (1968). Measurements and interpretation of low-energy photoelectrons. Jour. Geophys. Res. 73, 4199-4212.

Sheridan, W. F., Oldenberg, O., O., and Carleton, N. P. (1971). Excitation of nitrogen by fast protons and electrons. Jour. Geophys. Res. 76, 2429-2436.

Simpson, F. R. and McConkey, J. W. (1969). Excitation of the $A^2\Pi_u$ state of N_2^+ by electrons. Planet. Space Sci. 17, 1941-1948.

Skubenich, V. V. (1968). Excitation of molecular oxygen by low energy electrons. Opt. Spect. 25, 90-91.

Stanton, P. N. and St. John, R. M. (1969). Electron excitation of the first negative and Meinel bands of N_2^+. Jour. Opt. Soc. Amer. 59, 252-260.

Stein, J. A. and Walker, J. C. G. (1965). Models of the upper atmosphere for a wide range of boundary conditions. Jour. Atmos. Sci. 22, 11-17.

Stolarski, R. S. (1972). Analytic approach to photoelectron transport. Jour. Geophys. Res. 77, 2862-2870.

Stolarski, R. S. and Johnson, N. P. (1972). Photoionication and photo-absorption cross sections for ionospheric calculations. Proc. of the conference on theoretical ionospheric models, Pennsylvania State Univ., Ionospheric Res. Sci. Rept. no. 401, 219-236.

Stolarski, R. S., Dulock, V. A., Jr., Watson, C. E., and Green, A. E. S. (1967). Electron impact cross sections for atmospheric species. 2. Molecular nitrogen. Jour. Geophys. Res. 72, 3953-3960.

Takayanagi, K. and Itikawa, Y. (1970). Elementary processes involving electrons in the ionosphere. Space Sci. Rev. 11, 380-450.

Walker, J. C. G. (1965). Analytic representation of upper atmosphere densities based on Jacchia's static diffusion models. Jour. Atmos. Sci. 22, 462-463.

Watson, C. E., Dulock, V. A., Jr., Stolarski, R. S., and Green, A. E. S. (1967). Electron impact cross sections for atmospheric species. 3. Molecular oxygen. Jour. Geophys. Res. 72, 3961-3966.

Yngvesson, K. O. and Perkins, F. W. (1968). Radar Thomson scatter studies of photoelectrons in the ionosphere and Landau damping. Jour. Geophys. Res. 73, 97-110.

FIGURES

Figure 1. Energy spectrum of the primary photoelectrons at selected altitudes at dawn [$\chi = 90°$] (adapted from calculations by Stolarski 1972, private communication).

Figures 2a - 2c. Photoelectron pitch angle and energy spectra at selected altitudes at dawn. For negative values of μ [μ = cosine (pitch angle)] the electrons are moving in the downward direction, while for positive values they are moving upward. Note the pitch angle isotropy at low altitudes (a,b) and upward-downward unisotropy at high altitudes. Also, note the broadening and shifting towards lower energies of the spectrum features around 25 eV with decreasing $|\mu|$ at high altitudes and, also, the difference in the sign of slopes of the upward and downward spectra at the low energy limit.

Figure 3. Photoelectron flux energy spectrum at dawn. Note the gradual smoothening of the spectrum with increasing altitude and, also, the broadening and shifting towards lower energies of the spectrum features around 25 eV.

Figure 4. Mean photoelectron flux energies: $\bar{E}_s$ is the mean energy of the primary photoelectrons (source), top scale; $\bar{E}^-$ is the mean energy of the downward photoelectron flux, and $\bar{E}^+$ that of the upward, bottom scale. The curve to the right represents the ratio $\bar{E}^+/\bar{E}^-$. The mean photoelectron flux energy $\bar{E}_\Phi$ follows closely the $\bar{E}^+$ curve. Note that while the mean energy of the primary photoelectrons increases with decreasing altitude, the mean energy of the steady-state photoelectron flux decreases.

Figure 5. Pitch angle distribution of the total (integrated over all energies) photoelectron flux. Note the large upward-downward anisotropy above 500 km.

Figure 6. Photoelectron flux energy spectrum at noon. Note the rapid transition in the smoothness of the spectrum at about 300 km, and the broadening and shifting of the spectrum features with increasing altitude (compare with Figure 3).

Figure 7. Energy spectra of the upward flux at selected altitudes at noon. The shift and broadening of the features at 22.5 eV, and the energy dependent attenuation of the flux with increasing altitude, are clearly seen in this figure.

Figure 8. Mean energy of the steady-state photoelectron flux at noon as function of altitude and pitch angle cosine.

Figure 9. Total photoelectron fluxes at dawn and noon. Note the upward-downward flux unisotropy above about 250 km.

Figure 10. Comparison between calculated and measured photoelectron flux energy spectra at 180 km.

Figure 11. Comparison between calculated and measured photoelectron flux energy spectra at selected altitudes between 120 and 180 km.

Figure 12. Comparison between calculated and measured photoelectron flux energy spectra at selected altitudes between 120 and 303 km.

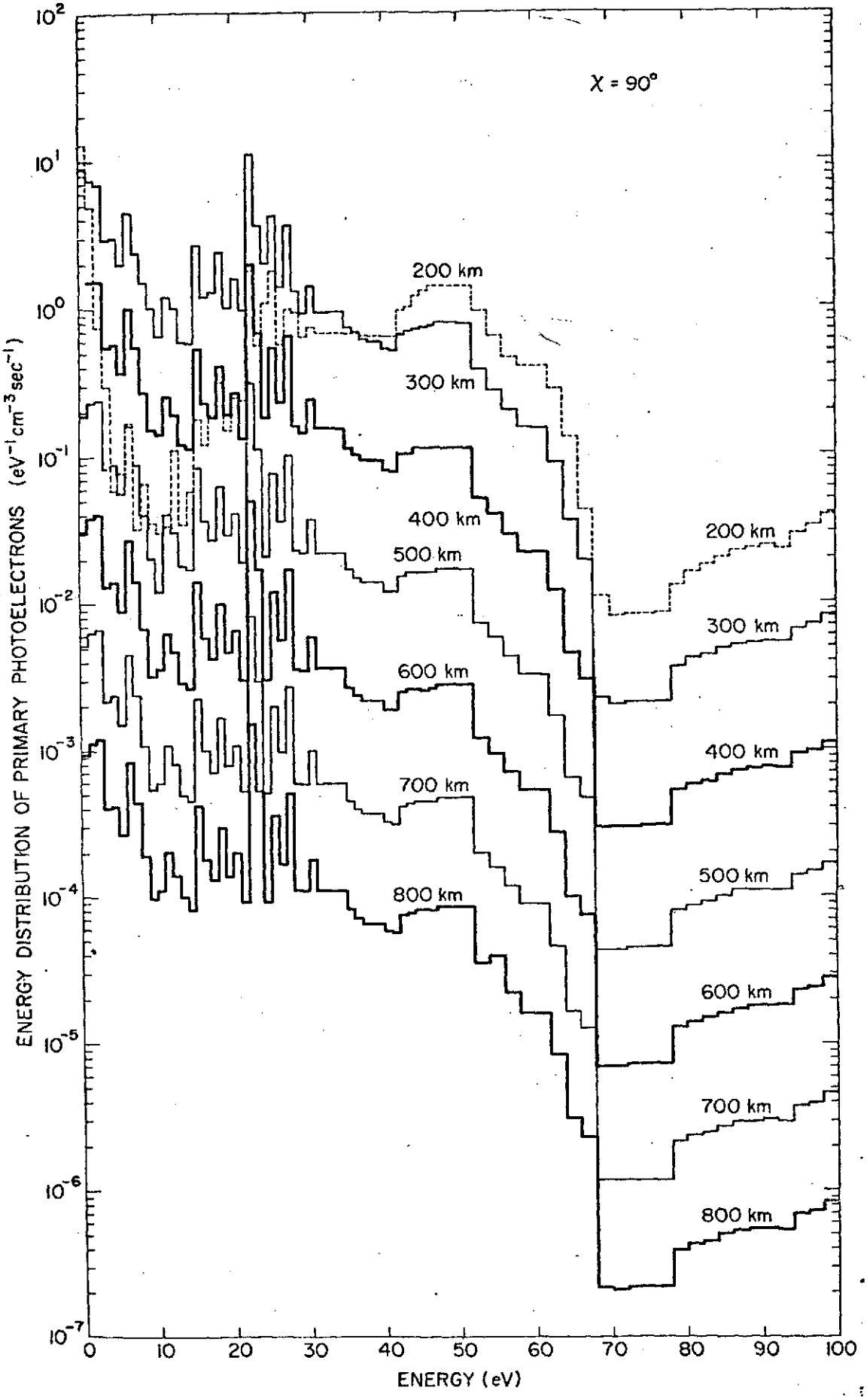
χ = 90°
200 km
300 km
400 km
500 km
600 km
700 km
800 km
200 km
300 km
400 km
500 km
600 km
700 km
800 km
ENERGY DISTRIBUTION OF PRIMARY PHOTOELECTRONS (eV⁻¹cm⁻³sec⁻¹)
ENERGY (eV)
10²
10¹
10⁰
10⁻¹
10⁻²
10⁻³
10⁻⁴
10⁻⁵
10⁻⁶
10⁻⁷
0
10
20
30
40
50
60
70
80
90
100

Figure 1

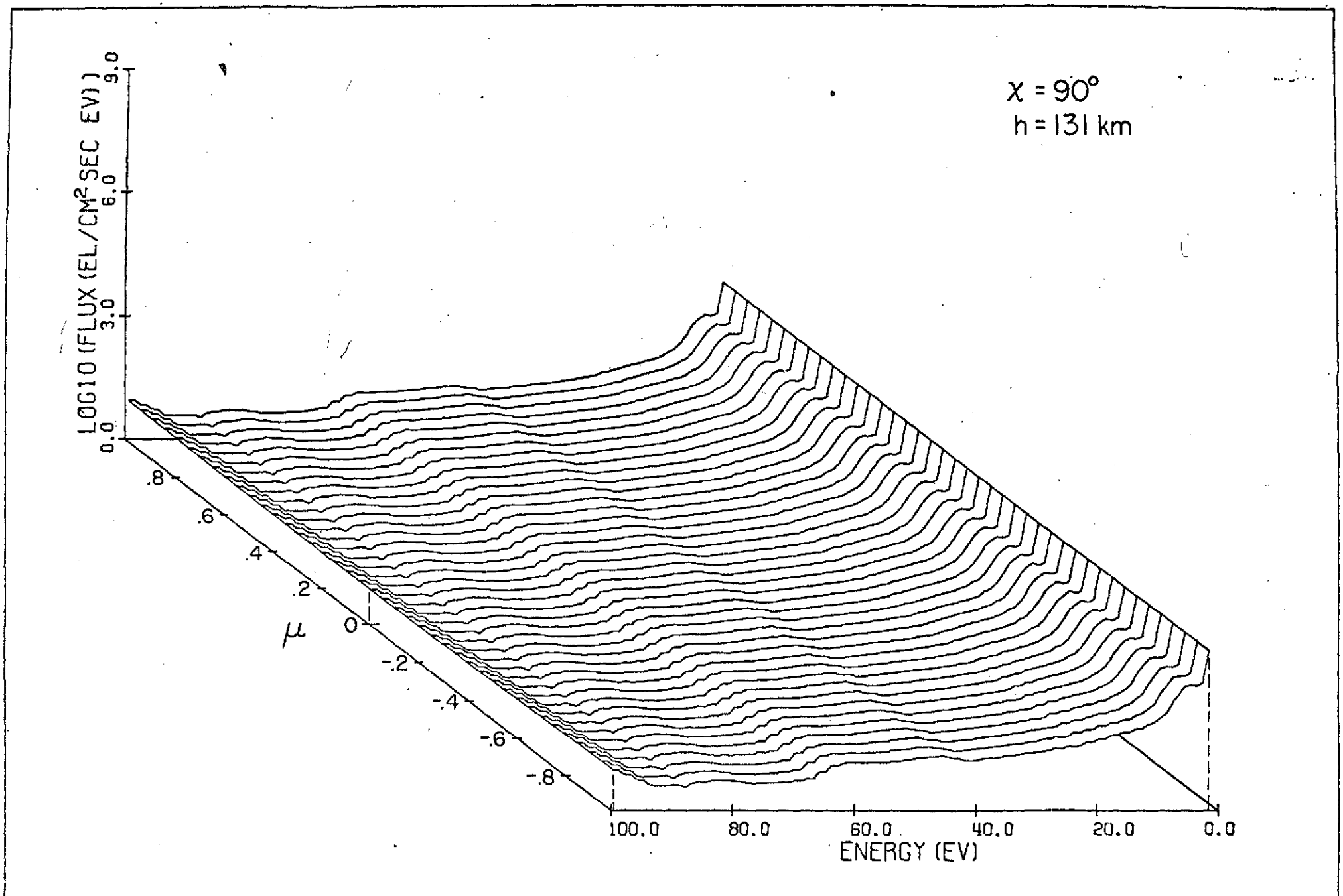
χ = 90°
h = 131 km
LOG10 (FLUX (EL/CM² SEC EV))
9.0
6.0
3.0
0.0
.8
.6
.4
.2
μ
0
-.2
-.4
-.6
-.8
100.0
80.0
60.0
40.0
20.0
0.0
ENERGY (EV)

Figure 2a

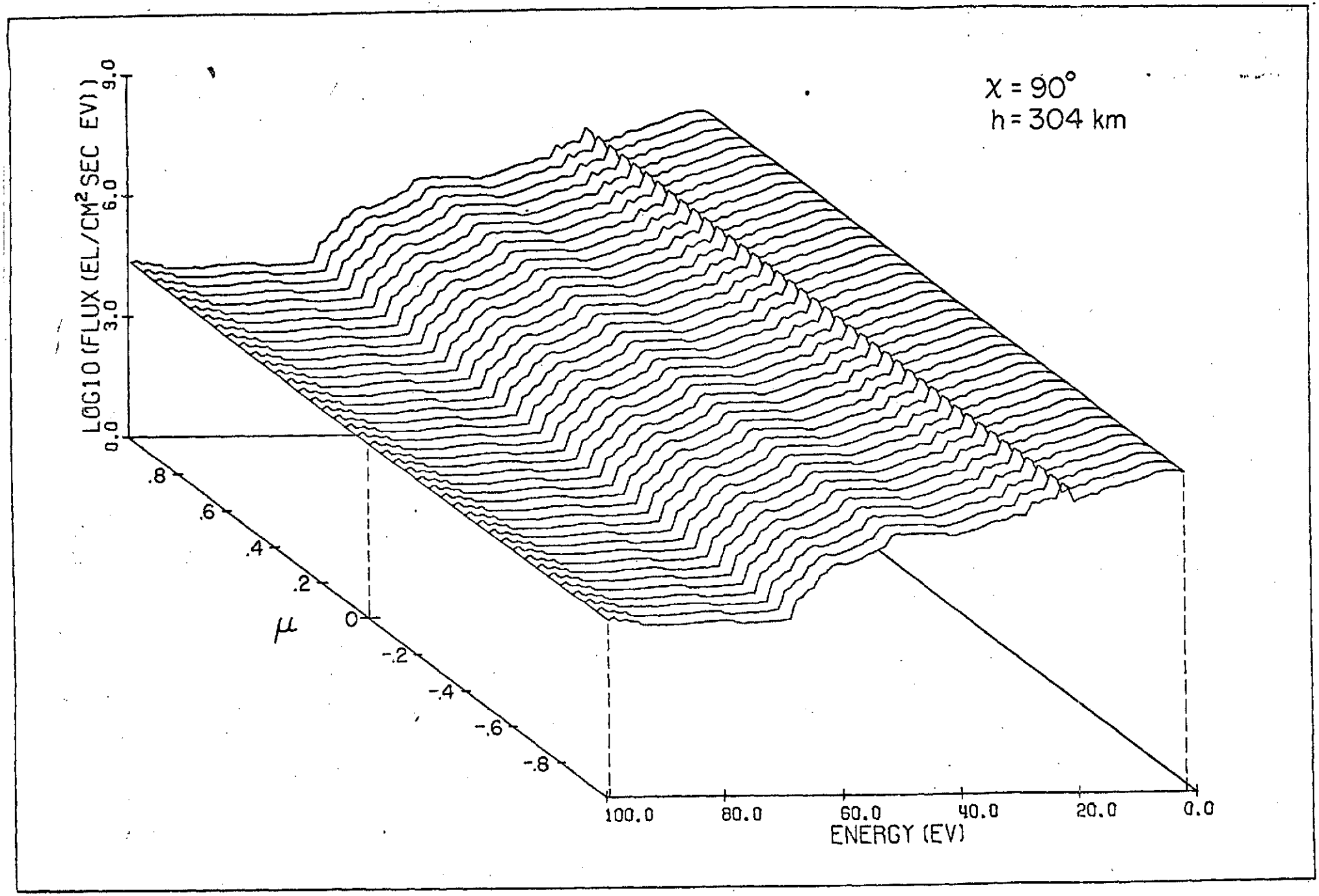
χ = 90°
h = 304 km
LOG10 (FLUX (EL/CM² SEC EV))
9.0
6.0
3.0
0.0
.8
.6
.4
.2
μ
0
-.2
-.4
-.6
-.8
100.0
80.0
60.0
40.0
20.0
0.0
ENERGY (EV)

Figure 2b

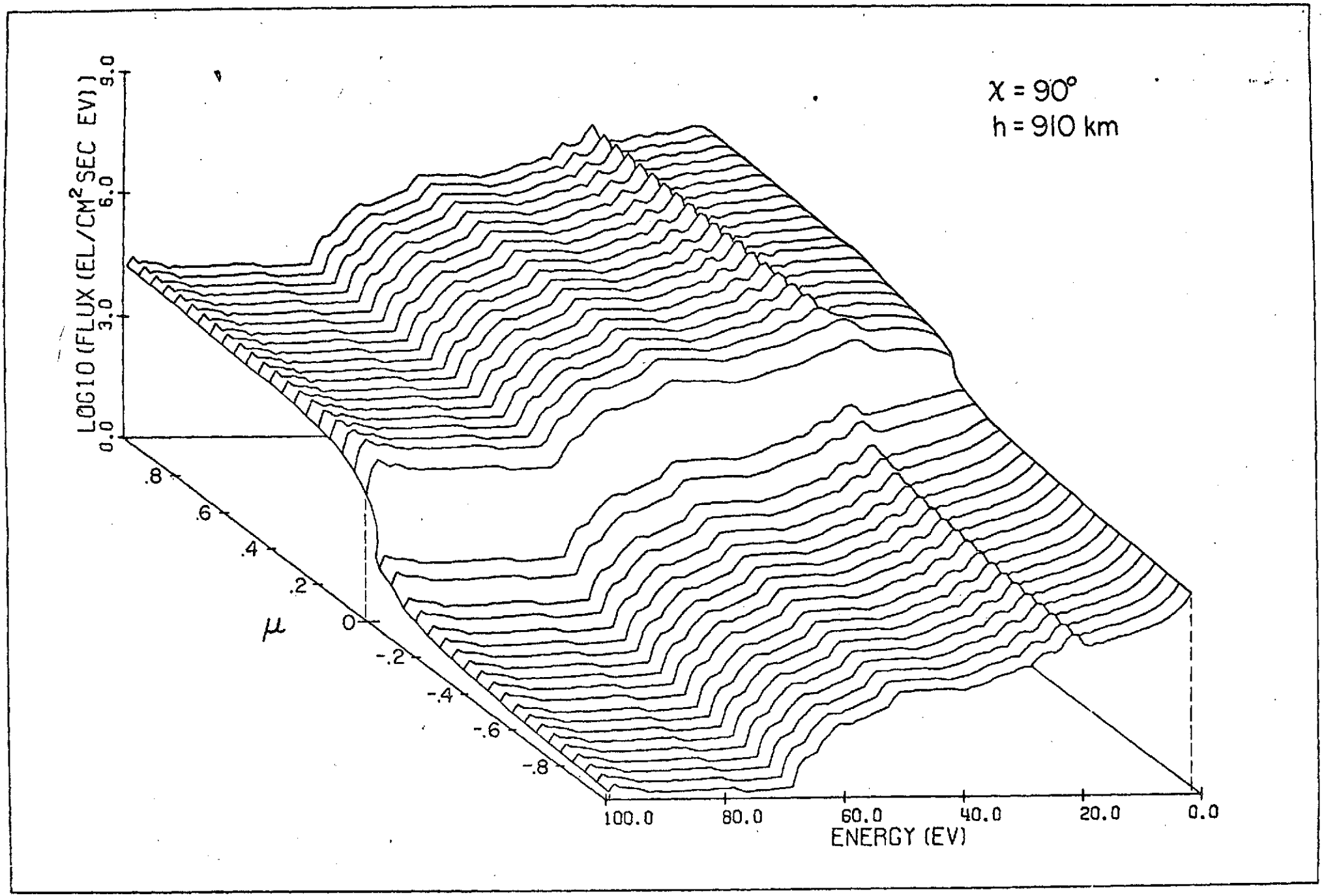
χ = 90°
h = 910 km
LOG10 (FLUX (EL/CM² SEC EV))
9.0
6.0
3.0
0.0
.8
.6
.4
.2
0
-.2
-.4
-.6
-.8
μ
100.0
80.0
60.0
40.0
20.0
0.0
ENERGY (EV)

Figure 2c

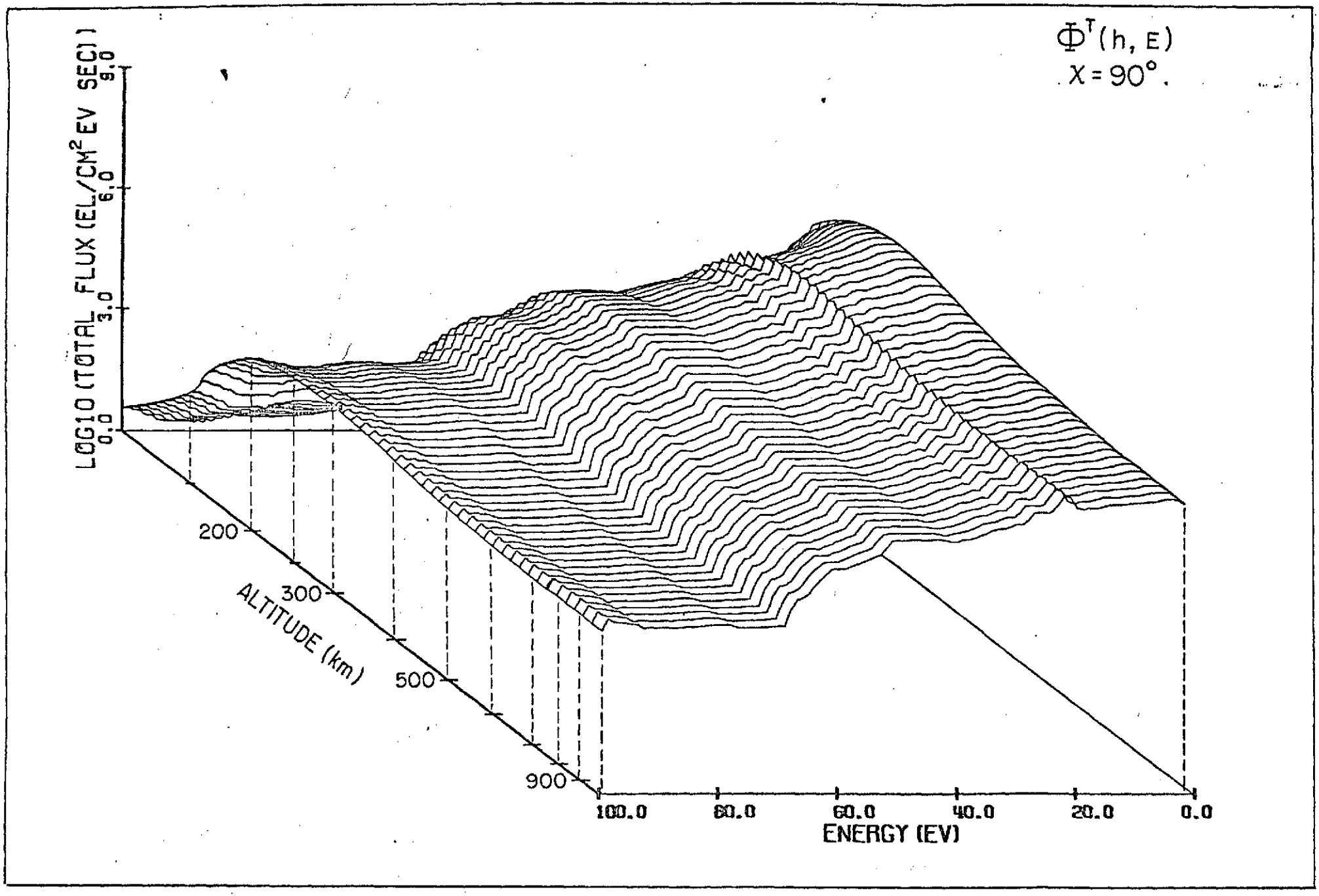
$\Phi^T(h, E)$
$\chi = 90°$.
LOG10 (TOTAL FLUX (EL/CM^2 EV SEC))
0.0
3.0
6.0
9.0
200
300
500
900
ALTITUDE (km)
100.0
80.0
60.0
40.0
20.0
0.0
ENERGY (EV)

Figure 3

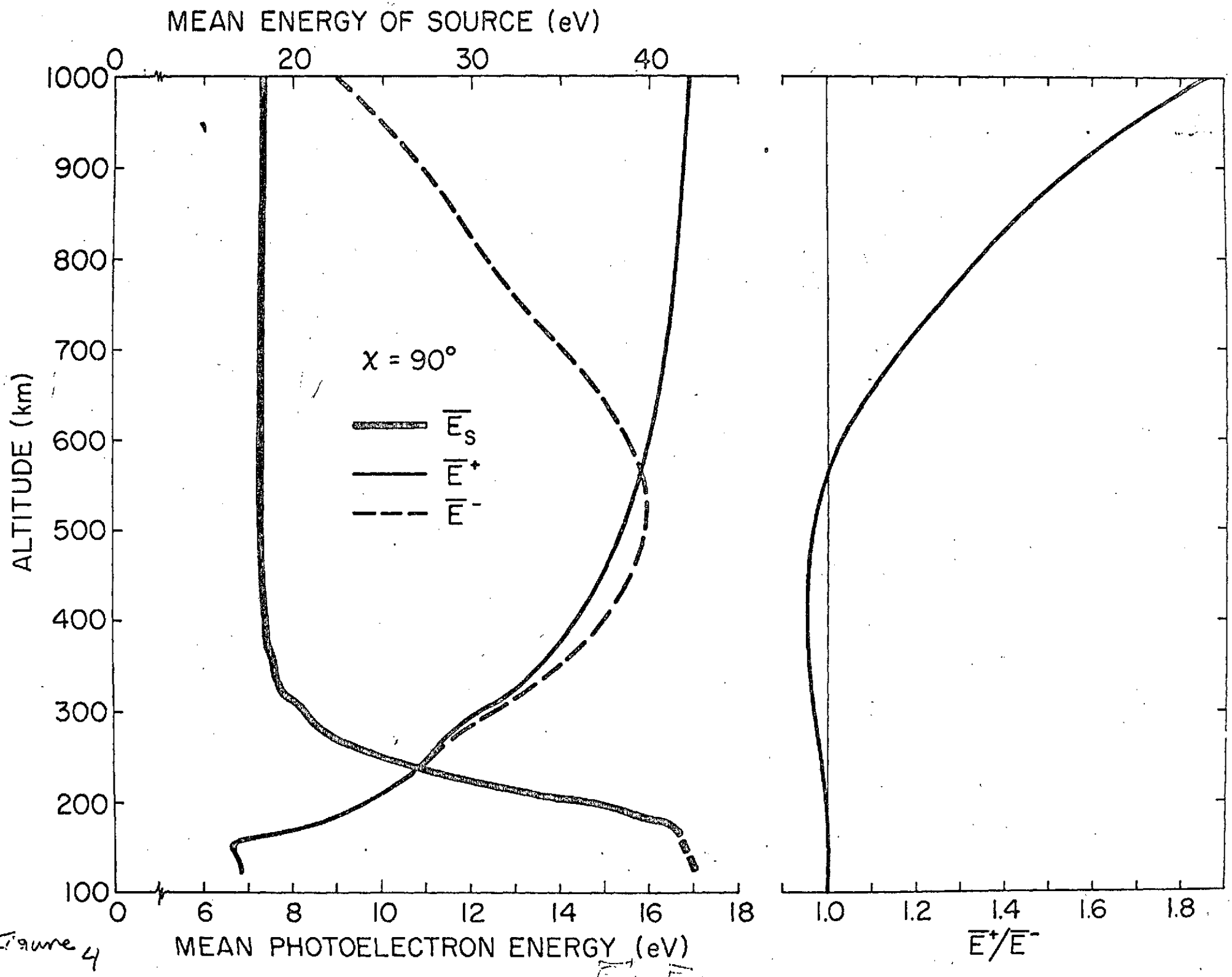
MEAN ENERGY OF SOURCE (eV)
0
20
30
40
1000
900
800
700
600
500
400
300
200
100
ALTITUDE (km)
χ = 90°
$\overline{E_s}$
$\overline{E^+}$
$\overline{E^-}$
0
6
8
10
12
14
16
18
MEAN PHOTOELECTRON ENERGY (eV)
$\overline{E}$ or $\overline{E^-}$
1.0
1.2
1.4
1.6
1.8
$\overline{E^+}/\overline{E^-}$

Figure 4

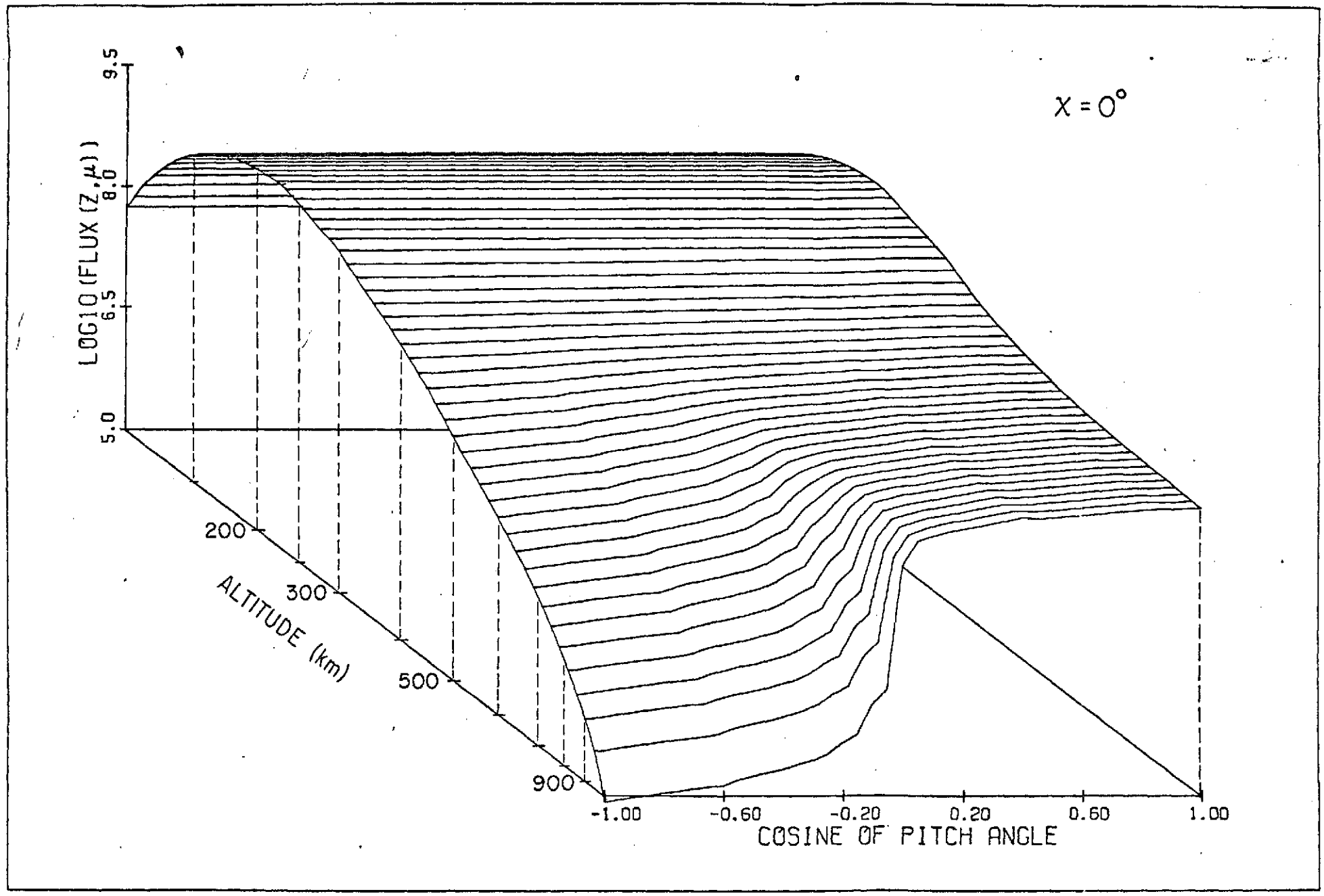
χ = 0°
LOG10 (FLUX (Z,μ))
9.5
8.0
6.5
5.0
200
300
500
900
ALTITUDE (km)
-1.00
-0.60
-0.20
0.20
0.60
1.00
COSINE OF PITCH ANGLE

Figure 5

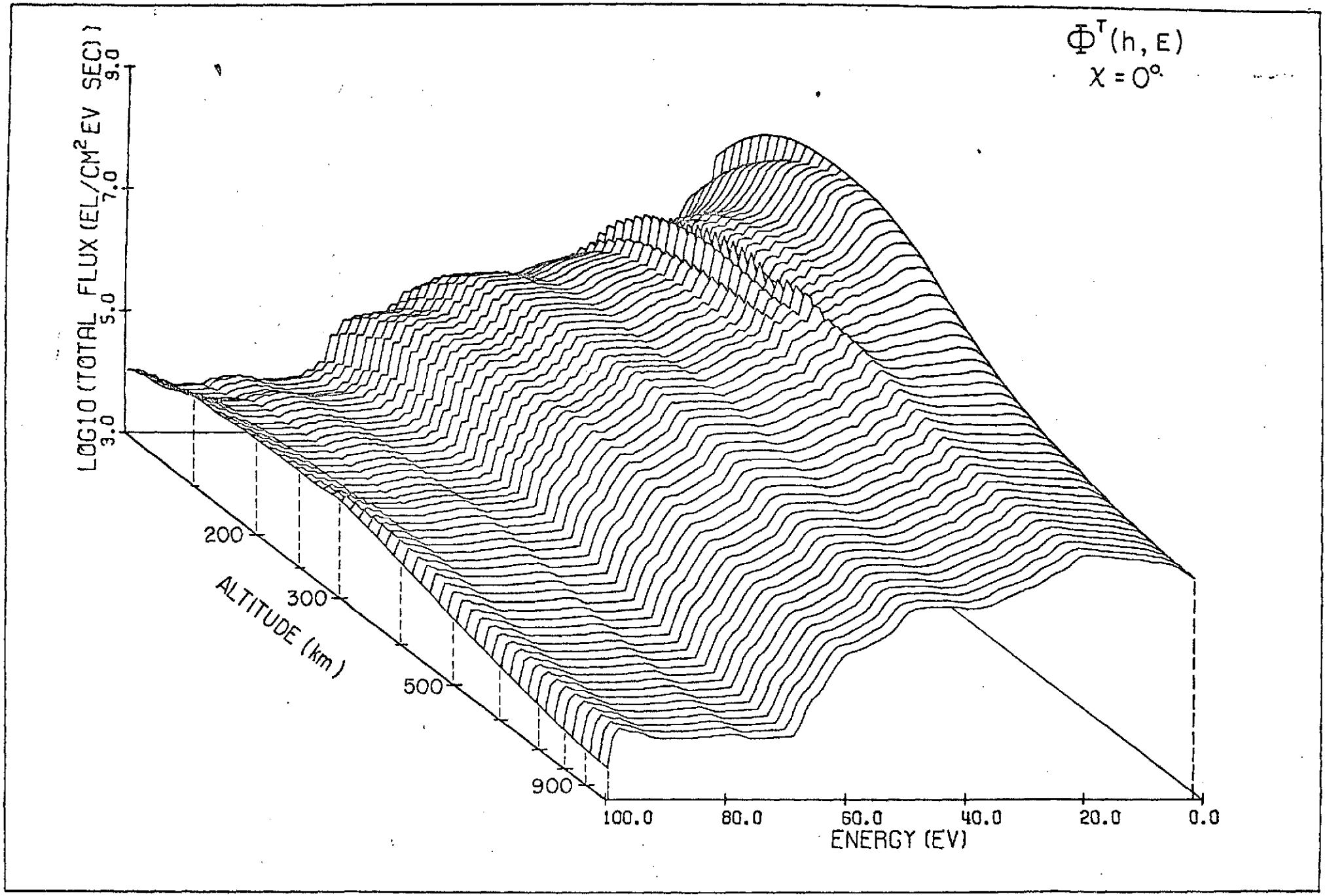
$\Phi^T(h, E)$
$\chi = 0°$
LOG10 (TOTAL FLUX (EL/CM^2 EV SEC))
9.0
7.0
5.0
3.0
200
300
500
900
ALTITUDE (km)
100.0
80.0
60.0
40.0
20.0
0.0
ENERGY (EV)

Figure 6

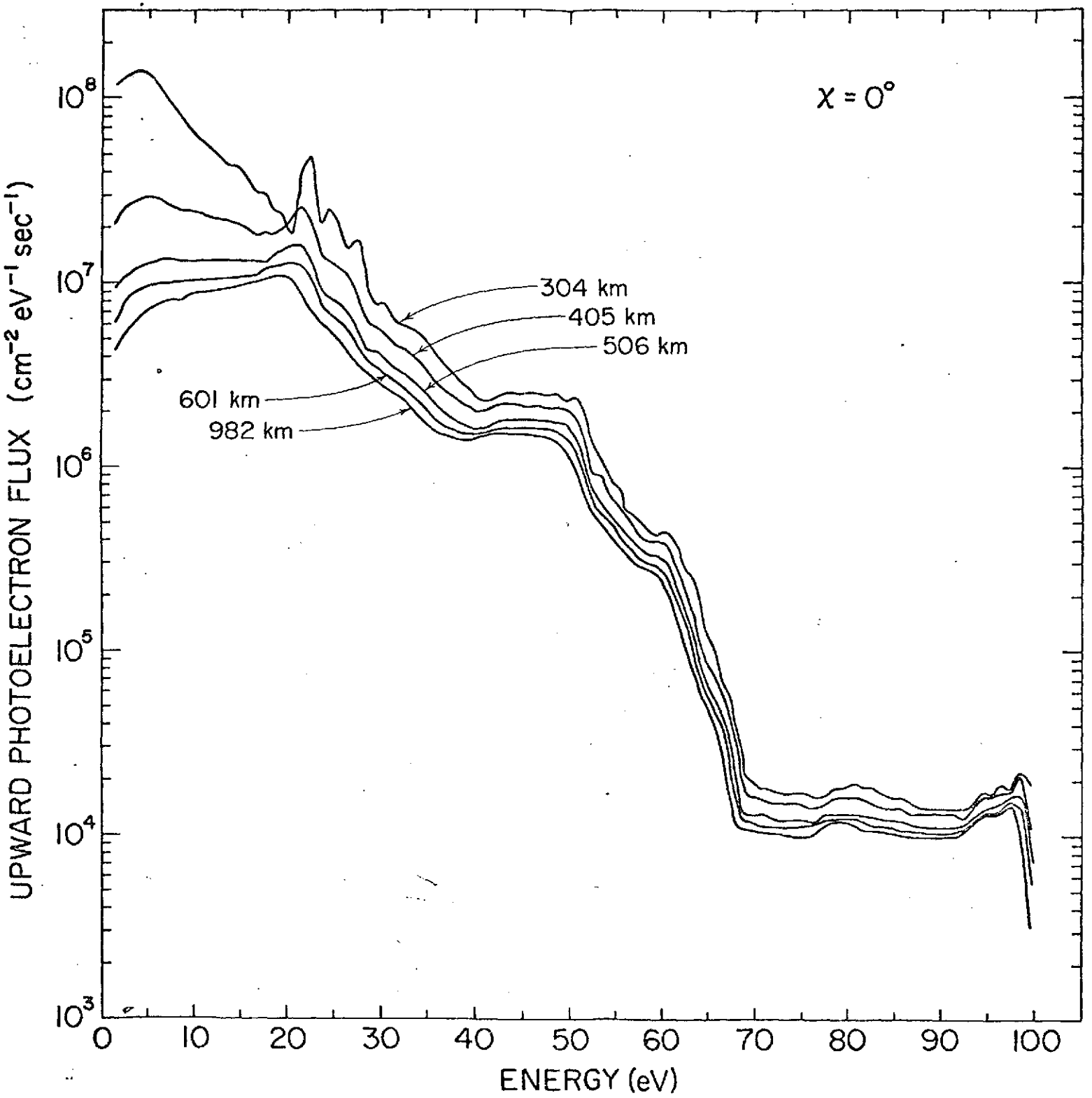
χ = 0°
304 km
405 km
506 km
601 km
982 km
UPWARD PHOTOELECTRON FLUX (cm⁻² eV⁻¹ sec⁻¹)
ENERGY (eV)
10⁸
10⁷
10⁶
10⁵
10⁴
10³
0
10
20
30
40
50
60
70
80
90
100

Figure 7

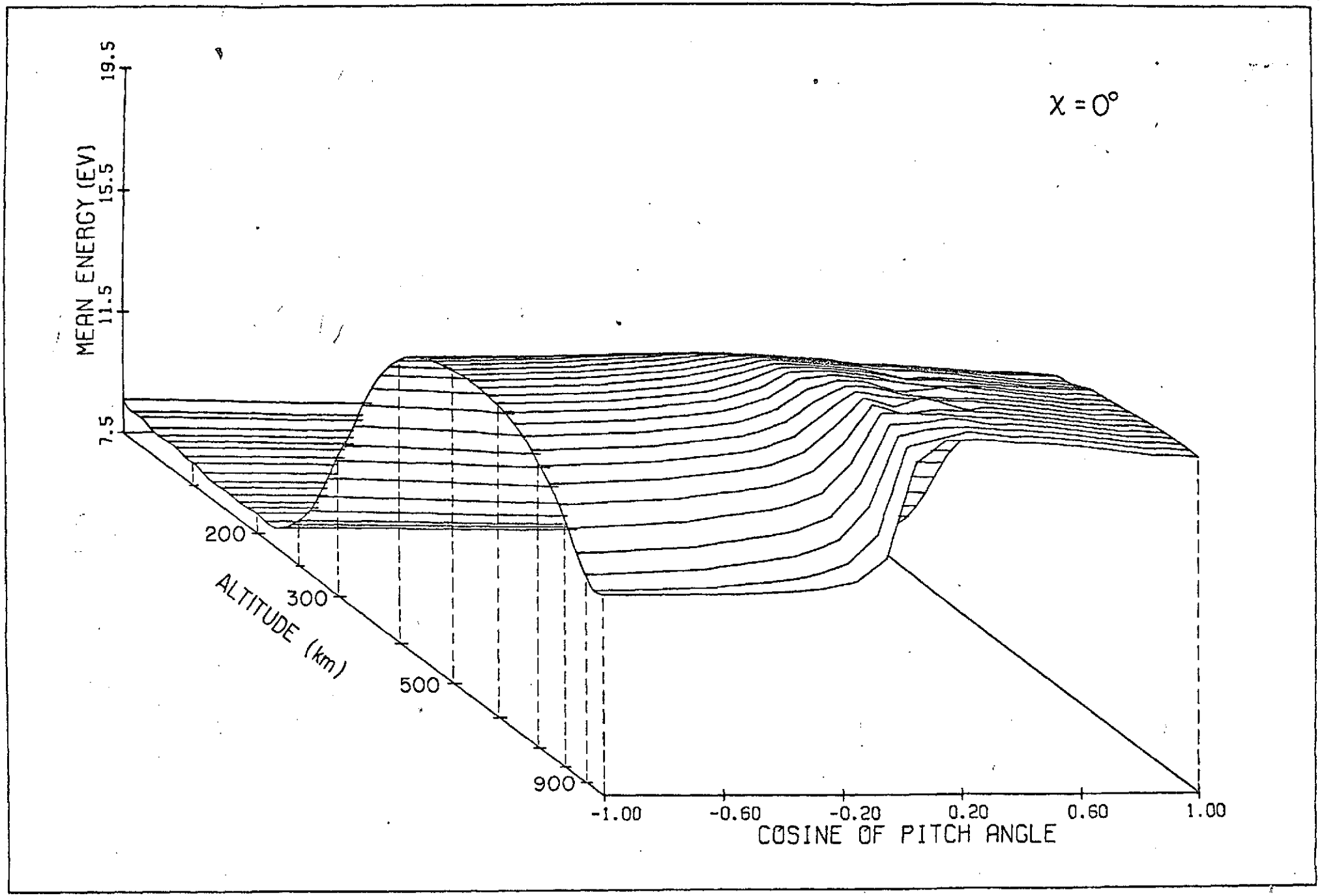
χ = 0°
MEAN ENERGY (EV)
19.5
15.5
11.5
7.5
200
300
500
900
ALTITUDE (km)
-1.00
-0.60
-0.20
0.20
0.60
1.00
COSINE OF PITCH ANGLE

Figure 8

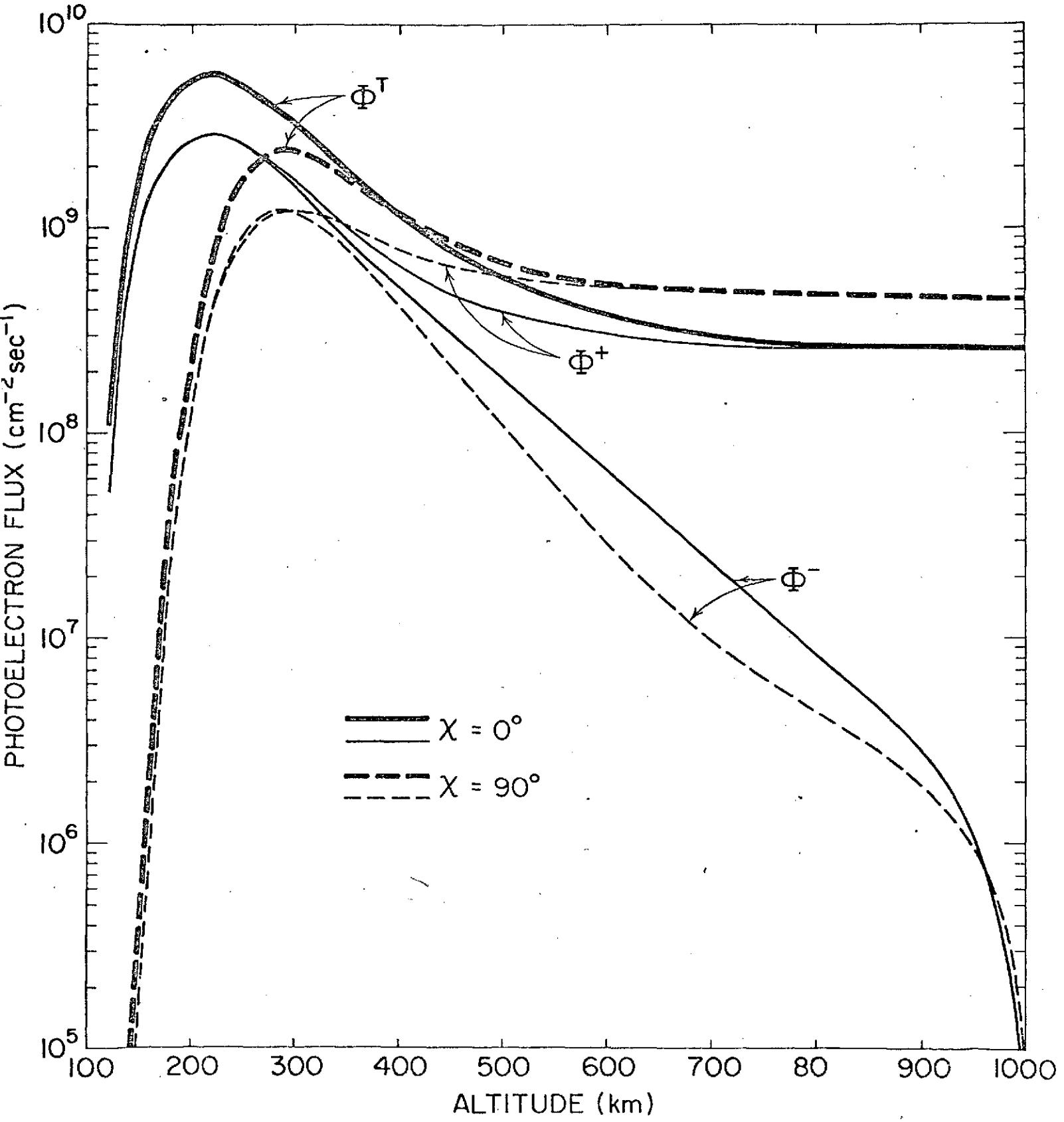
10^{10}
10^{9}
10^{8}
10^{7}
10^{6}
10^{5}
PHOTOELECTRON FLUX ($cm^{-2}sec^{-1}$)
Φ^T
Φ^+
Φ^-
$\chi = 0°$
$\chi = 90°$
100
200
300
400
500
600
700
80
900
1000
ALTITUDE (km)

Figure 9

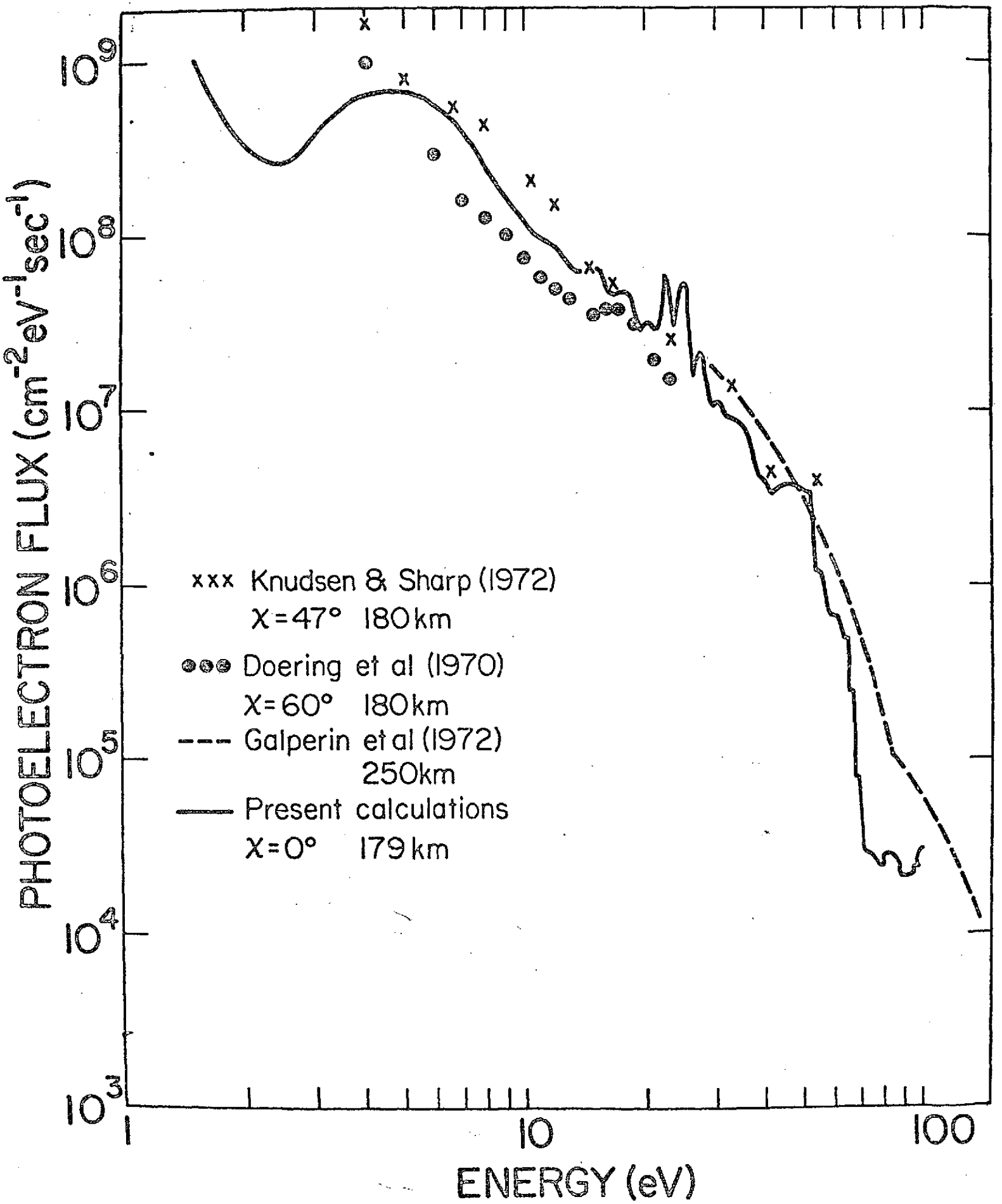
PHOTOELECTRON FLUX (cm^{-2}eV^{-1}sec^{-1})
10^9
10^8
10^7
10^6
10^5
10^4
10^3
1
10
100
ENERGY (eV)
xxx Knudsen & Sharp (1972)
χ=47° 180km
●●● Doering et al (1970)
χ=60° 180km
--- Galperin et al (1972)
250km
—— Present calculations
χ=0° 179 km

Figure 10

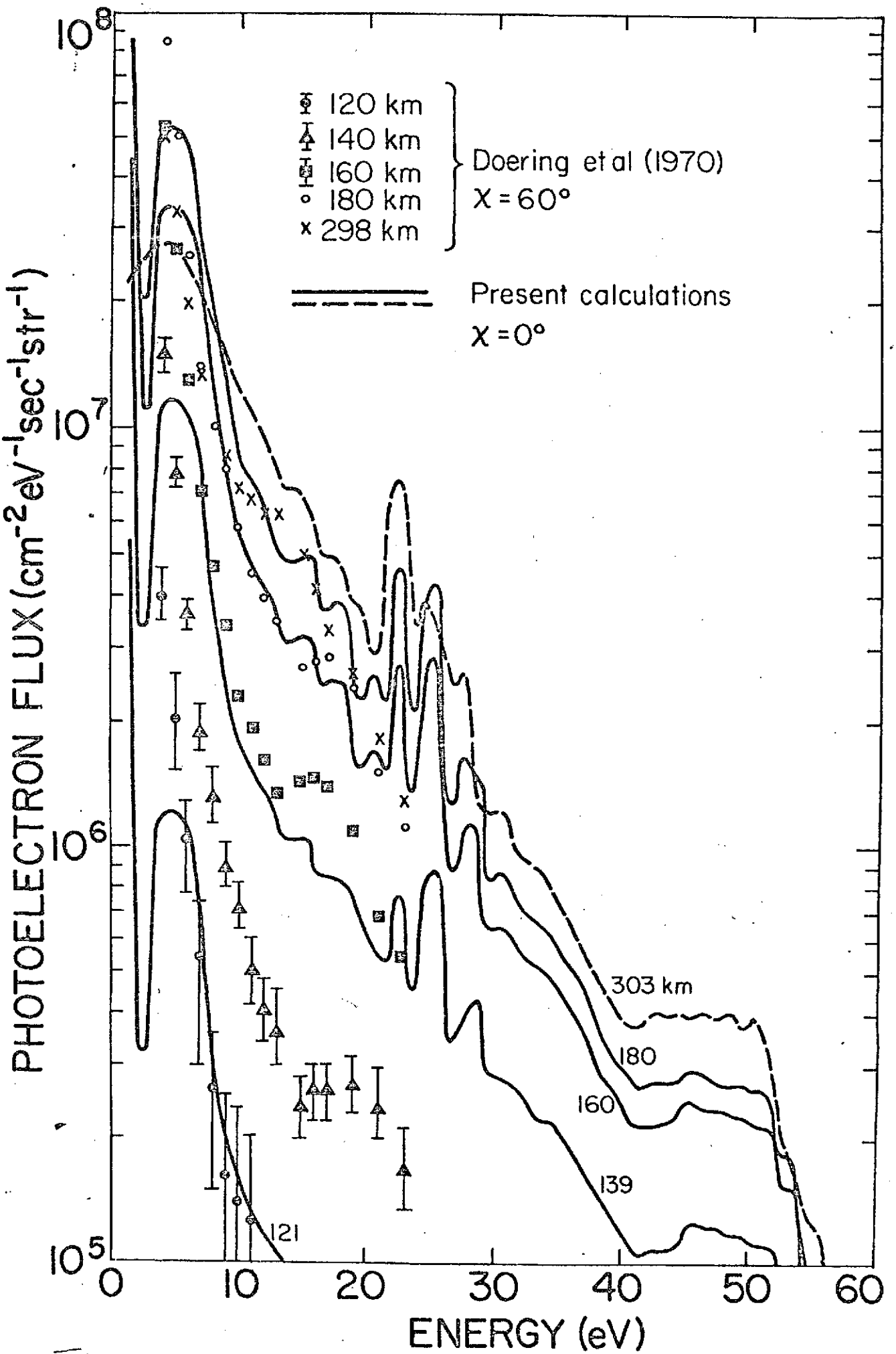
120 km
140 km
160 km
180 km
298 km
Doering et al (1970)
χ = 60°
Present calculations
χ = 0°
303 km
180
160
139
121
PHOTOELECTRON FLUX (cm⁻²eV⁻¹sec⁻¹str⁻¹)
ENERGY (eV)
10⁸
10⁷
10⁶
10⁵
0
10
20
30
40
50
60

Figure 11

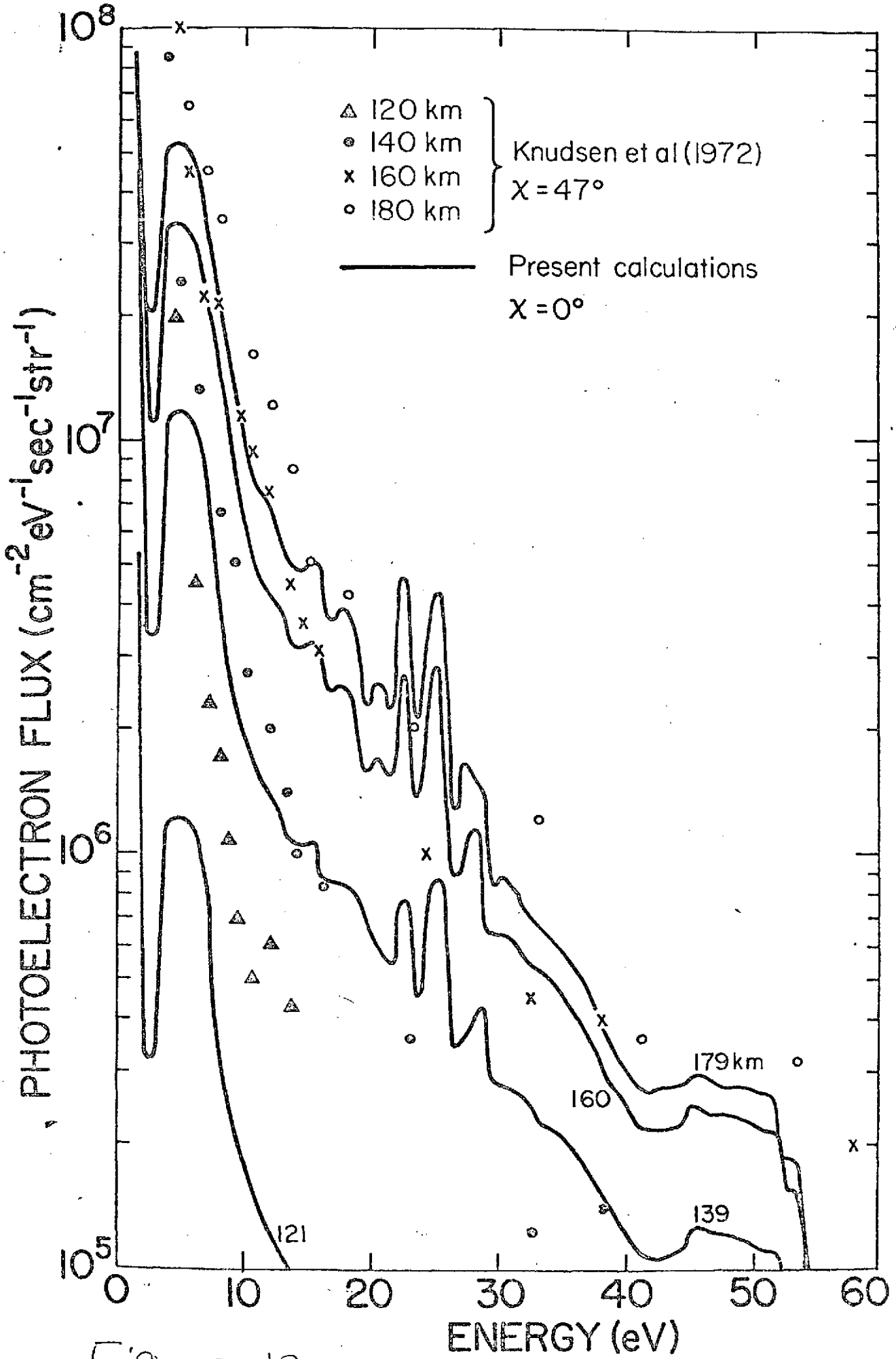
120 km
140 km
160 km
180 km
Knudsen et al (1972)
χ = 47°
Present calculations
χ = 0°
179 km
160
139
121
PHOTOELECTRON FLUX (cm⁻² eV⁻¹ sec⁻¹ str⁻¹)
ENERGY (eV)
10⁸
10⁷
10⁶
10⁵
0
10
20
30
40
50
60

Figure 12